Carbohydrate Polymers 117 (2015) 34–42

Contents lists available at ScienceDirect

Carbohydrate Polymers

journal homepage: www.elsevier.com/locate/carbpol

Gold nanoparticles in the engineering of antibacterial and anticoagulant surfaces☆

Heike M.A. Ehmann[a,b], Doris Breitwieser[a], Sascha Winter[b], Christian Gspan[c], Günther Koraimann[a], Uros Maver[d], Marija Sega[e], Stefan Köstler[f], Karin Stana-Kleinschek[g], Stefan Spirk[b,g,*], Volker Ribitsch[a]

[a] Institute for Chemistry, University of Graz, Graz, Austria
[b] Institute for Chemistry and Technology of Materials, Graz University of Technology, Graz, Austria
[c] Institute for Electron Microscopy and Fine Structure Research, Centre for Electron Microscopy Graz, Graz, Austria
[d] Faculty of Medicine, University of Maribor, Maribor, Slovenia
[e] Center of Transfusion Medicine, University Medical Centre Maribor, 2000 Maribor, Slovenia
[f] Joanneum Research Materials, Institute for Surface Technologies, 8160 Weiz, Austria
[g] Institute for the Engineering and Design of Materials, University of Maribor, Maribor, Slovenia

ARTICLE INFO

Article history:
Received 27 May 2014
Received in revised form 22 August 2014
Accepted 25 August 2014
Available online 22 September 2014

Keywords:
Chitosan sulfate
Gold nanoparticles
Anticoagulant activity
Antimicrobial surfaces
Quartz crystal microbalance

ABSTRACT

Simultaneous antibacterial and anticoagulant surfaces have been prepared by immobilization of engineered gold nanoparticles onto different kinds of surfaces. The gold nanoparticle core is surrounded by a hemocompatible, anticoagulant polysaccharide, 6-*O* chitosan sulfate, which serves as reduction and stabilizing agent for the generation of gold nanoparticles in a microwave mediated reaction. The particle suspension shows anticoagulant activity, which is investigated by aPTT and PT testing on citrated blood samples of three patients suffering from congenital or acquired bleeding disorders. The amount of nanoparticles deposited on the surfaces is quantified by a quartz crystal microbalance with dissipation unit. All gold containing surfaces exhibit excellent antimicrobial properties against the chosen model organism, *Escherichia coli* MG 1655 [R1-16]. Moreover, blood plasma coagulation times of the surfaces are increased after deposition of the engineered nanoparticles as demonstrated by QCM-D.

1. Introduction

In the past years, silver containing antimicrobial materials have reentered the focus in the engineering of medical materials. In particular, the increasing amounts of multi resistant bacteria strains, which are very often involved in hospital acquired infections (HAI, ca. 4 Mio./year in the EU), are a threat to modern societies (ECDC, 2012). While these strains are not more infectious than non-resistant ones, an effective treatment is very often difficult and leads to complications and in severe cases even to death (37,000 year^{-1} in the EU). The origins of these resistances are manifold and include careless use and prescription of antibiotics. Usually, the time span until new resistances of bacteria toward antibiotics are developed covers a few years (e.g. penicillin: mass production started in 1943, first observation of resistant strains in 1947), in a few cases even some tens of years (Davies & Davies, 2010). Nevertheless, the ability of bacteria to handle and to tolerate antibiotics after a certain period of time can be simplified in first glance as a form of evolutionary process, As a consequence, the cells develop tolerance leading to the evolution of resistances. In the beginning of antibiotic exposure, all non-resistant bacteria are killed while the resistant ones survive and multiply. In fact, resistant bacteria are much older than man-made antibiotics and the reservoir of antimicrobial strains in the environment is underestimated so far (D'Costa, McGrann, Hughes, & Wright, 2006).

However, very recently this rather general sight on the topic was related to so called persister bacterial cells. These persisters are phenotypic variants of normal cells, but they are mostly dormant and inactive. Therefore, antimicrobial agents do not kill these cells and tolerances leading to resistances are developed. In addition, the formation of biofilms buries the persister cells making them even more difficult to treat (Conlon et al., 2013).

☆ Members of the European Polysaccharide Network of Excellence and NAWI Graz.

* Corresponding author at: University of Technology Graz, Institute for Chemistry and Technology of Materials, Stremayrgasse 9, 8010 Graz, Austria. Tel.: +43 31687332284.
E-mail address: stefan.spirk@tugraz.at (S. Spirk).

http://dx.doi.org/10.1016/j.carbpol.2014.08.116
0144-8617/

In contrast, there are hardly any bacterial strains known, which exhibit resistance against silver, despite the exposure of bacteria to non-inhibitory silver levels for more than 4 billion years (Alexander, 2009). This can be related to the rather unspecific mode of action, which interferes many enzymatic key processes (also those in persisters) taking place in microorganisms (Lara, Garza-Treviño, Ixtepan-Turrent, & Singh, 2011). Therefore, Ag in different kind of forms (bulk-metal, ionic, nanoparticles) is used in the coating/composition of medical materials such as wound dressings for instance (Alexander, 2009). However, one of the drawbacks of silver is its low (photo)chemical stability and it is the origin of argyria, an illness related to massive silver intake, which limits its use in several areas of medical devices. An alternative to silver is gold since it is assumed to exhibit high chemical stability and inertness under physiological conditions. This stability makes gold an attractive target in many areas of research in life sciences, biomedicine and materials sciences. Applications of gold nanoparticles as drug carriers in e.g. cancer therapy, as diagnostic tools in fluorescent tomography or as antimicrobial component have been described recently (Khan, Vishakante, & Siddaramaiah, 2013).

Since materials equipped with gold (nanoparticles, NPs) feature antimicrobial activity, they are very attractive for the design of antimicrobial surfaces. It is known that the mode of action of gold nanoparticles (AuNPs) against microorganism is very similar to those of silver NPs (Bhattacharya & Mukherjee, 2008). In addition, the use of bio- and hemocompatible polysaccharides as capping/stabilizing agents (Cheng, Betts, Kelly, Schaller, & Heinze, 2013; Sacarescu, Simionescu, & Sacarescu, 2011) for NPs allows for applying them in materials where simultaneous anticoagulant activity is required (Breitwieser et al., 2013a,b; Croes, Stobberingh, Stevens, Knetsch, & Koole, 2011; Huang & Yang, 2004).

The use of natural anticoagulants such as heparin for this purpose imposes the risk of infections in case cGMP are not strictly followed since heparin is currently obtained from vertebrates. For this reason, it is highly desirable to replace heparin against semi-synthetic anticoagulants such as sulfated celluloses and chitosans (Fasl et al., 2010; Gericke et al., 2011). Although the specific mode of interaction of heparin in the blood coagulation cascade via a pentasaccharide unit is probably hard to mimick using these semisynthetic compounds, research in this area may result in additives (either on surfaces or in solutions) enhancing the effects of heparin rather than replacing it. Another disadvantage of these semi-synthetic sulfated polysaccharides is that they do not provide broad-spectrum antibacterial activity. Even sulfated chitosans are not significantly active against a variety of microorganisms close to neutral pH values since the amine groups are blocked by the negatively charged sulfate groups (Fasl, Fras-Zemljic, Gössler, Stana-Kleinschek, & Ribitsch, 2012). As a consequence, these polysaccharides are not capable to inhibit the growth of (multi-resistant) strains, which would be highly desirable later on in materials that come into contact with blood. Since these sulfated polysaccharides have been successfully deposited on artificial blood vessels (e.g. PET), there is a large potential in case antimicrobial activity can be incorporated into this class of polysaccharides.

In this paper, we aim at addressing this problem by encapsulating gold nanoparticles in an anticoagulant sulfated chitosan polymer. There are several questions that must be envisaged starting from the applicability of the chosen polysaccharide for nanoparticle preparation, the anticoagulant activity of nanoparticles in suspensions and their behavior, when they are adsorbed onto surfaces in terms of antibacterial and anticoagulant activity. Since an extensive study on all of the parameters would go beyond scope of a single paper, selected tests will be performed in order to assess the suitability of the chosen approach in order to prepare *simultaneous* antibacterial and anticoagulant surfaces. In order to tackle these questions, the paper is structured as follows: (i) Detailed characterization of the nanoparticles size and charge in order to validate the presence of a sulfated chitosan shell around a gold core. (ii) Determination of the anticoagulant activity of the gold nanoparticle suspension using aPPT and PT tests on patients suffering from clotting diseases. (iii) Immobilization of the nanoparticles onto cellulosic surfaces and quantification using a quartz crystal microbalance. (iv) Determination of antibacterial activity against a model organism (gram negative one, *Escherichia coli* MG 1655 [R1-16]) and estimation of anticoagulant activity of blood plasma on the surfaces.

2. Experimental

2.1. Materials

$HAuCl_4 \cdot 3H_2O$ (>99.99%) was obtained from Alfa Aesar (Karlsruhe, Germany). For the dissolution of $HAuCl_4 \cdot 3H_2O$, MilliQ water was used ($\Omega \leq 18{\cdot}2\ \mu\Omega$). Sulfated chitosan was prepared from hydrolyzed chitosan (M_w ca. 20 kDa, degree of deacetylation according to producer: 85%, prepared from low molecular weight chitosan (source: crab shells, Batch No. 13604PC) from Sigma Aldrich by refluxing in 1 M HCl under nitrogen atmosphere, followed by adjustment to pH 5.8 using 2 M NaOH, subsequent dialysis and lyophilization) and $ClSO_3H$ under reflux in DMF according to a literature procedure (Fasl et al., 2010). Sulfated chitosan with a DS_S of 0.86 and a M_w of ca. 10 kDa was obtained after sulfation. The molecular weight was determined by using an Ubbelohde viscosimeter with a diameter of 0.24 mm which was placed in a thermostat ($T = 20\,^{\circ}C$). The reduced viscosity η_{red} was determined according to the relation $\eta_{red} = \frac{(t_{sample}/t_{solvent})-1}{c_{sample}}$ whereby t_{sample} is the time which was needed for the different concentrations to pass the marks, $t_{solvent}$ is the time needed for the water to pass the marks and c_{sample} is the corresponding concentration in mg/ml. The reduced viscosity was plotted as a function of the sample concentration and extrapolated to zero concentration. The intercept of the linear plot is the intrinsic viscosity $[\eta]$. The calculation of M_w was performed using the *Mark–Houwink*–Sakurada equation

$$[\eta] = K \times M_w^a$$

The used values for the coefficients K (4.97×10^{-5}) and a (0.77) were determined by Vikhoreva et al. (2005) for sulfated chitosan with a sulfur content of 14–15%.

The degree of deacetylation (83%) of the sulfated chitosan was determined by conductometric titration: 2 ml of 1% (w/w) aqueous sulphated chitosan solution was pipetted into a titration vessel. 1 ml of 100 mM HCl was also added to adjust the pH to about pH 3. At this pH value all amino groups protonate into positively charged NH_3^+ groups which behave as a weak acid in the analytic solution and can be titrated with a base titrant (KOH). The vessel was then filled up with distilled water to a volume of 40 ml. A Mettler Toledo T70 titrator, with a 10 ml burette, was used for the incremental addition of 100 mM KOH as the titrant. Increments of 0.1 ml were added in a timed interval within 10–60 s. An equilibrium criteria of 0.1 μS/10 s was set. The equivalence points were evaluated with the "slope" method. The equivalence points correspond to the crossing points of the titration curve slopes.

EDC·HCl (1-ethyl-3,3-dimethylaminopropyl carbodiimide hydrochloride, 98%) was obtained from Sigma. CMC (carboxymethyl cellulose, M_w 90,000, DS_{COONa}: 0.7) and PEI (high molecular weight) were purchased from Sigma Aldrich. Trimethylsilyl cellulose with a DS_{Si} of 2.55, (M_w = 175,000, M_n = 36,000, kindly provided by the Centre of Excellence for Polysaccharide Research, University of Jena) was used for cellulose model film preparation (Koehler, Liebert, & Heinze, 2008). Blood

plasma for QCM-D studies and $CaCl_2$ (medical grade) were purchased from Siemens Healthcare Diagnostics Products, Marburg, Germany.

Citrated blood samples were obtained by clean venipuncture using 19-ga butterfly needles and Monovette tubes (Sarstedt, Nürmbrecht, Germany) containing 1/9 vol. of 0.106 M Na-citrate. Plasma was prepared by double centrifugation (1500 × *g*, each for 10 min, at room temperature) and was stored in polypropylene tubes at −70 °C until use.

2.2. Preparation of Au@S-Chi NPs using microwave assisted heating

The reduction of $HAuCl_4 \cdot 3H_2O$ and subsequent formation of S-Chi coated nanoparticles was carried out in Biotage Eight microwave reactors. The reactions were performed in sealed microwave-assisted synthesis process vials dedicated and designed for the single-mode microwave system. In a typical procedure, 2 ml of an aqueous S-Chi solution (10 mg/ml) and 1 ml $HAuCl_4 \cdot 3H_2O$ (5 mM, dissolved in water) are placed in a 10 ml microwave vial and heated at 100° for 8 min under stirring using microwave irradiation. Since S-Chi is a reducing polysaccharide additional reducing agents are not required.

2.3. Transmission electron microscopy (TEM)

Bright field images were acquired on a Tecnai F20 transmission electron microscope with a Schottky Field Emission Gun (FEG) from FEI operating at 200 kV. The energy filtered images were recorded with a post column energy filter (Gatan Imaging Filter, GIF) on a 2k × 2k CCD with the software DigitalMicrograph. The samples were prepared by bringing 2–3 drops of the solution from the ground material onto a holey carbon film. This carbon grid was dried at room temperature and after that used for the TEM investigation. For analytical information about the nanoparticles the energy dispersive X-ray spectroscopy (EDX) was utilized with an energy dispersion of 0.01 keV. The EDX system has an Si(Li) detector from the company EDAX.

2.4. Small angle X-ray scattering (SAXS)

The SAXS experiments were performed using the S3-MICROpix solution of Hecus with a 50 W microsource Genix 2009 from Xenocs. The tube consists of a copper anode with an emission wavelength of 1.5418 Å for the K_α line. The sample to detector distance was 291 mm with an angle of 4.2°. The optics are 3D for point focus with a beam size of $50 \times 200\ \mu m^2$ and a flux up to 4×108 photons/s/mm^2. The point focus at the detector has a monochromatic SAXS resolution of $q(\min) \geq 4 \times 10^{-3}$ Å^{-1}. The scattering vector (q) range is between 0.003 Å^{-1} and 1.9 Å^{-1}.

As detection system, a 2D Pilatus 100k Dectrics Detector 34×84 mm^2, with a pixel size of $172 \times 172\ \mu m^2$ was used. A Nickel filter was used as semitransparent primary beam stop.

The samples were sealed in quartz glass mark tubes of Hilgenberg with a linear adsorption coefficient of 75.8 cm^{-1} for Cu$K\alpha$-radiation. The outer diameter of the mark tubes was 1.0 mm with a wall thickness of 0.01 mm. The samples were irradiated with 50 kV and 1 mA emission current for 1200 s. The background measurement was done for 1200 s but with closed shutter.

The data evaluation and correction were performed using the software program PDH (Primary Data Handling) from the PCG software package version 3.01.10.1 The generalized indirect Fourier transformation was performed using the software program GIFT (Generalized Indirect Fourier Transformation from the PCG software package version 3.01.10) (Bergmann et al., 1999; Bergmann, Fritz, & Glatter, 2000; BrunnerPopela & Glatter, 1997; Fritz, Bergmann, & Glatter, 2000; Weyerich, Brunner-Popela, & Glatter, 1999). The Lagrange multiplier was determined using the interval from λ = 10 to 0, whereas the search was performed in 0.25 steps which corresponds to 41 Lagrange multipliers. To obtain 201 equidistant points in the r-scale, 20 cubic B-splines were used as basic functions. As minimization algorithm, the Boltzmann simplex simulated annealing algorithm with a start annealing temperature of 20 °C was used. The salt concentration was assumed to be 0.01 M and the volume fraction was kept constant in the calculations for the determination of the other two linearly dependent parameters (r, Z_{eff}). The structure factor for charged hard spheres via the rescaled mean sphere approximation (RMSA) can be calculated using the Yukawa potential ($V(r)$) in (20):

$$V(r) = \beta\upsilon(r) = \frac{z^2 e_0^2}{4\pi \in \in_0 kT} \times \frac{e^{-\kappa^{(a-2a)}}}{r(1+\kappa a)^2} \quad (1)$$

whereby z is the number of unit electron charges on the particle, e_0 is the unit charge of an electron, ε_0 is the permittivity of vacuum, ε the relative dielectric constant, k the Boltzmann constant, T the temperature, κ the Debye screening parameter, a the radius of a sphere, r the center to center distance of the spheres, the thermodynamic $\beta = 1/kT$ with k being the Boltzmann constant and $\nu(r)$ the interaction potential.

This method leads to stable pair distance distribution functions, but in order to derive the correct structure factor only two of the three parameters (radius, charge, volume fraction) are varied due to the linear dependence of the results, which is represented as the direct correlation function $c(r)$:

$$c(r) = -\beta\upsilon(r) \quad (2)$$

2.5. Activated partial thromboplastin time (aPTT) testing

aPTT was assayed using a tilt tube technique. A kaolin–inosithin suspension (10 mg/ml kaolin, 0.5 mg/ml inosithin) in isotonic barbiturate acetate (BA) buffer, pH 7.35, was used as the aPTT reagent. The regular testing was performed using 100 μl of pre-warmed plasma and 100 μl of kaolin-inosithin suspension, which were pre-incubated in a glass tube at 37 °C. After pre-incubation (standard pre-incubation time (PIT = 1 min)), 100 μl of pre-warmed (37 °C) 0.0025 M $CaCl_2$ was added and the clotting time was recorded in seconds. For the testing of the prepared samples, the regular procedure was upgraded with the addition of either 25 or 50 μl of the nanoparticle suspension (c = 0.1 mg/ml) to the blood plasma.

2.6. PT testing

The PT (prothrombin time) was assayed using a tilt test tube technique. Blood plasma samples were mixed with Tissue Factor (TF) (containing phospholipid) at 37 °C and an excess of calcium chloride (25 mM) was added to initiate coagulation. The time taken from the addition of calcium to the formation of the fibrin clot was recorded as PT. For the clotting testing plasma from three different patients (with different clinical diagnoses) was withdrawn. The results of clotting times after the addition of two different volumes of the nanoparticle suspension, were compared to the aPTT and PT for the plasma without the added suspension.

2.7. Gram-negative antibacterial surface activity evaluation

All experiments were performed under sterile conditions in three repetitions. All buffer, media, and *E. coli* MG 1655 [R1-16] cultures were prepared according to literature protocols (Miller, 1977; Wagner, Zahrl, Rieser, & Koraimann, 2009; Zahrl, Wagner, Bischof, & Koraimann, 2006). The test surfaces were sterilized using ethanol (Roth Karlsruhe, Germany), and fixed at the bottom of

12-well plates. 2 ml of bacterial culture (*E. coli* MG 1655 [R1-16] cultivated in M9 medium) were added (OD_{600} was set to 0.03) to each sample, and the plates were incubated for 12 h (37 °C, shaking with 180 rpm). Then, the bacterial suspension was removed, and the samples were rinsed extensively with PBS buffer (150 mM sodium chloride and 150 mM sodium hydrogen phosphate, pH 7.4, salts purchased from Roth Karlsruhe, Germany) in order to remove loosely attached bacteria. In order to cultivate bacteria attached to the sample surface, 2 ml fresh M9 medium was added to each sample, followed by incubating for 12 h at 37° C. Finally, the samples were extensively rinsed with buffer as described above, and analyzed using scanning electron microscopy (SEM, Carl Zeiss FE-SEM SUPRA 35 VP electron microscope, acceleration voltage: 10 kV). The samples were dried under continuous gas flow over night, fixed on SEM sample holders, and sputtered with gold/platinum (Jeol JFC-1100 E ion sputter, operating at $D = 10$ mA).

2.8. QCM-D experiments, immobilization of S-Chi@Au on the substrates and determination of their anticoagulant properties

QCM-D experiments are performed using a QCM-D E4 from Q-Sense (Gothenburg, Sweden). For every run, three sensors have been monitored in parallel. For QCM measurements, Au coated QCM sensors (GSX301, from Q-Sense, Gothenburg, Sweden) with a resonance frequency of 5 MHz were used. The QCM-sensors were decorated with a thin layer (d: 25 ± 1 nm) of cellulose according to recently published procedures (Mohan et al., 2012, 2013) and further incubated for 30 min with 100 μl CMC solution ($c = 2$ mg/ml) and dried in a steady stream of nitrogen.

Two different approaches were used for immobilization of S-Chi@Au on the CMC surfaces referred to as EDC, and PEI. For all immobilization experiments, aqueous solutions of EDC ($c = 0.078$ mmol/l), and PEI ($c = 20$ mmol/l, 0.5 M KCl) were used. The CMC surfaces were incubated with these solutions for 15 min followed by rinsing with MilliQ water to remove the reversibly bound material from the surface and drying in a stream of N_2. All adsorption experiments involving S-Chi@Au were performed using a QCM-D under continuous flow conditions at a flow rate 0.1 ml/min for 60 min ($T = 21.0 \pm 0.1$ °C), followed by a rinsing step with MilliQ water to remove reversibly bound material from the surface. The amount of particles on the surface can be determined by calculating the difference of the frequencies before and after S-Chi@Au adsorption according to the Sauerbrey equation(Sauerbrey, 1959) (3), where Δm denotes the adsorbed mass, $\Delta f_n/n$ is the frequency shift at the corresponding overtone and C is the Sauerbrey constant (=−17.7 ng/ cm^2/Hz for a 5 MHz sensor).

$$\Delta m = C\frac{\Delta f_n}{n} \tag{3}$$

The determination of anticoagulant properties and clot formation was performed according to literature (Andersson et al., 2005; Doliska et al., 2012) in an open QCM-D cell made from PTFE which was designed and manufactured in the institute's workshop. For these experiments, following surfaces were used: CMC, EDC, PEI, S-Chi@Au (EDC), and S-Chi@Au (PEI). Surface modified QCM sensors were mounted in the open measurement cell, and equilibrated to 37.0 ± 0.1 °C. Then, citrated normal blood plasma (ORKE 41, 100 μl) was equilibrated to 37.0 °C and placed onto the crystal. After ca. 2 min coagulation was triggered by addition of 100 μl 0.025 M $CaCl_2$ (equilibrated to 37.0 °C). All experiments were performed on three sensors for each surface modification. The frequency and dissipation change as a function of time provides information about the onset time, fibrin deposition rate and total coagulation time. A more detailed description of the test set-up can be found elsewhere (Doliska et al., 2012).

3. Results and discussion

As a precursor for the gold nanoparticles, $HAuCl_4$ is used, which is reduced by sulfated chitosan using microwave assisted heating. Recently, the reducing nature of this polysaccharide has been discussed, which can be related to its aldehyde end groups (Breitwieser et al., 2013b; Fig. 1).

The nanoparticle synthesis was optimized in terms of heating time, temperature and the S-Chi:$AuCl_4$ ratio. The reaction was monitored by UV–vis spectroscopy, which is widely used in such syntheses to monitor the surface plasmon resonance of gold nanoparticles. It allows for a rough estimation of the size of the nanoparticles by analysis of the position of λ_{max} (Schlücker, 2009). In the case of S-Chi@Au NPs, the position of λ_{max} is observed at 530 nm, which indicates a particle radius of approximately 13 nm. While UV-VIS gives a first impression about the size of the particles, additional methods must be employed for particle characterization since the plasmon resonance is not only sensitive to size but also to the shape and environment of the nanoparticles. For this purpose, (HR-)TEM images have been acquired, which show that the spherical particles have an average geometric diameter of approximately 15 nm (Fig. 2). In addition, these particles are highly crystalline but the sulfated chitosan shell cannot be identified in the HR-TEM due to the large scattering contrast provided by the gold core. However, TEM/EDX clearly proves that the sulfated chitosan surrounds the gold core, because sulfur and nitrogen are detected in significant amounts. Moreover, the particles are highly negatively charged ($\zeta \equiv -35$ mV at pH 7) which is a proof for the presence of the negatively charged sulfated chitosan on the gold core. Besides these methods, small angle X-ray scattering was employed for the analysis of the nanoparticles. A very easy and convenient approach is to use the generalized inverse Fourier transformation (GIFT), which allows for the investigation of interacting nanoparticles (Bergmann et al., 2000; Ehmann et al., 2013).

In principle, SAXS in combination with GIFT offers several advantages: the data evaluation can be done for concentrated solutions/suspensions, it requires only a minimum amount of a-priori information, it is capable to determine form factors ($P(q)$) and structure factors ($S(q)$) simultaneously and the influence of particles with charged groups can be evaluated. Therefore, this procedure reflects 'real' conditions much better than TEM, where usually diluted solutions are used to coat the TEM grids. While particle dimensions are very similar to those derived from HR-TEM, the interaction of particles can be evaluated via $S(q)$. The decrease in intensity at low values of q clearly indicates repulsive interactions between the individual particles. Although the GIFT approach is capable to yield the thickness of shells in core–shell nanoparticles, the large scattering cross section of gold in combination with the high charge density on the S-Chi does not allow to provide precise statements on the thickness of the shell around the gold core (data not shown).

3.1. Clotting tests of blood plasma and S-Chi@Au

In order to evaluate whether the nanoparticle suspensions show any anticoagulant activity, they have been tested by aPTT and PT prior to immobilization on surfaces. In these tests, small volumes of S-Chi@Au are added to blood plasma obtained from patients suffering from different types of illnesses and aPTT and PT are determined. All three patients have in common that their disease increases their risk for thrombosis and blood vessel clotting. Therefore, a positive effect on these patients can give some rise to the potential and the power of our nanoparticle system in e.g. anticoagulant dosage therapy.

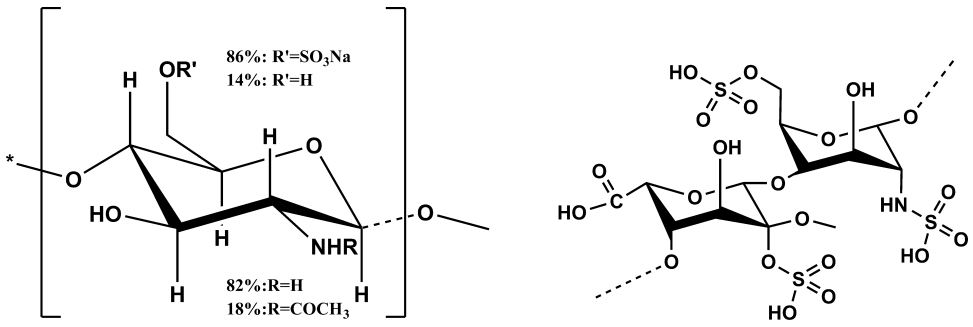

Fig. 1. Molecular structures of semi-synthetic 6-*O* chitosan sulfate and the natural anticoagulant heparin.

3.2. aPTT and PT testing

Prothrombin time (PT) and activated partial thromboplastin time (aPTT) are widely used laboratory tests to investigate the extrinsic and intrinsic pathways of coagulation. These tests are diagnostically performed for any patient suspected of having a coagulopathy. PT is most often used to monitor the effects of Warfarin-based oral anti-coagulant therapy for patients who are at higher risk for heart valve replacement, deep vein thrombosis, pulmonary embolism, coronary thrombosis or other thromboembolic diseases. aPTT is usually ordered to monitor the effects of unfractionated heparin therapy. It can be used to detect circulating anticoagulants such as Lupus anti-coagulant and anti-factor VIII. In addition, it detects congenital and acquired procoagulant deficiencies, except for Factor VII.

The aPTT of the investigated blood plasmas varies in a range from 32 to 36 s which is still in the normal range but at the lower limit (expected normal times: 30 to 50 s). Upon addition of a small volume (0.25 μl, $c = 0.1$ mg/ml) of S-Chi@Au to the corresponding blood plasma, the aPTT nearly doubles for all samples. An addition of an even bigger volume (0.50 μl, $c = 0.1$ mg/ml) of the nanoparticles suspension to the corresponding blood plasmas leads to a further increase in aPTT (Table 1).

A similar elongation of the clotting process is evident through the determination of the PT. For all used samples, these times are significantly increased. Increased aPTT and PT point at an effect on both, the intrinsic and extrinsic blood coagulation pathways, which means that a non-factor specific activity takes place. A possible explanation for the anticoagulant effect could be in the Ca^{2+} binding capacity of the amino and sulfate groups, which are present on the nanoparticle surface. In order to get deeper insights into the nature of these effects, additional testing with other added nanoparticle suspension volumes must be performed, while extra testing is required to understand the mechanism behind

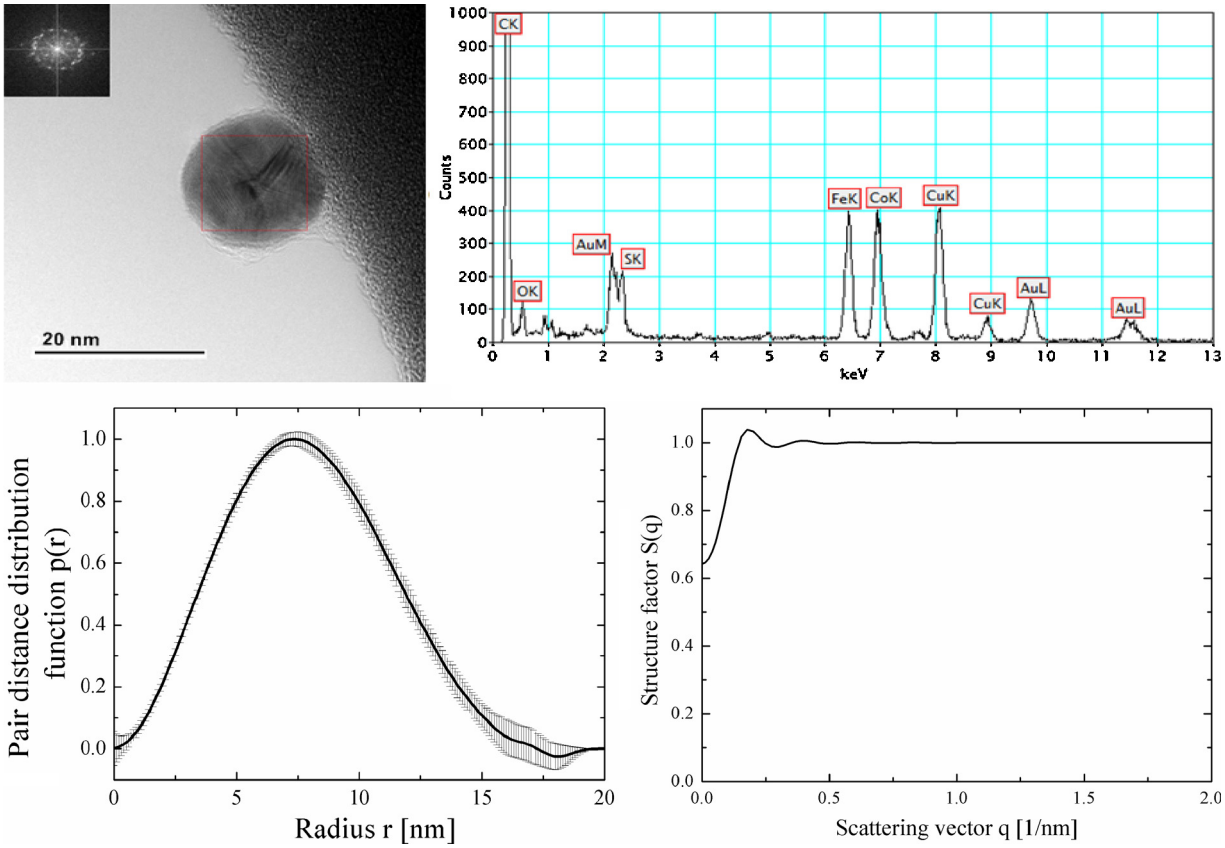

Fig. 2. Characterization of the nanoparticles using transmission electron microscopy/EDX analysis and small angle X-ray scattering. The estimated errors in the SAXS curve have been calculated by Monte-Carlo simulations.

Table 1
Overview on the results of clotting tests using S-Chi@Au using blood plasma of three patients suffering from different diseases. estimated errors <5%.

Sample	aPTT [s]	PT [s]
Patient 1—atherosclerotic heart disease of native coronary arteries		
Plasma 1 (P1)	33.5	12.7
P1 + 0.25 μl NPS	84.1	14.1
P1 + 0.50 μl NPS	103.8	15.4
Patient 2—ventriculi adeno calcification, intestinal type, her 2 negative, small curvature		
Plasma 2 (P2)	32.4	11.9
P2 + 0.25 μl NPS	69.3	13.1
P2 + 0.50 μl NPS	89.3	14.8
Patient 3—vomiting, epileptic seizures		
Plasma (P3)	36.0	10.2
P3 + 0.25 μl NPS	79.5	11.6
P3 + 0.50 μl NPS	117.7	13.5

coagulation prevention using such nanoparticle systems. Although these activities are planned, they go far beyond the scope of this paper and will be reported on another occasion. Even without additional testing, it is clear that these nanoparticles have potential for anticoagulant therapy or as new potential coatings for blood testing tubes instead of the most commonly used sodium citrate or heparin. Results are summarized in Table 1.

3.3. Immobilization on surfaces

Since the nanoparticles have shown promising results in anticoagulant testing of blood plasma, the next step is to immobilize them on surfaces in order to prepare simultaneous anticoagulant and antimicrobial materials. Different types of surfaces are capable to be modified with the AuNPs, whereby two practical approaches are chosen in this paper. As a substrate, carboxymethyl cellulose (CMC) is employed, which can be easily deposited on different types of surfaces e.g. by spin coating. In addition, CMC is negatively charged at pH 7 and the carboxylic groups can be exploited for further modification of the surfaces. Having these two facts in mind, two ways of modification can be followed. First, an electrostatic deposition of a cationic polymer (e.g. polyethyleneimine, PEI), which acts as a binder between the CMC surface and the negatively charged S-Chi@AuNPs. Second, conjugation via carbodiimide chemistry such as EDC can be realized, which is based on the reaction of a carboxylic group with the carbodiimide forming an isoacylurea intermediate, which in turn is capable to react with amine groups of the sulfated chitosan (Williams and Ibrahim, 1981). Both ways lead to surfaces that are modified with S-Chi@AuNPs and the amount of deposited particles can be determined using a quartz crystal microbalance with dissipation unit (QCM-D). The adsorption of the S-Chi@AuNPs can be followed online under flow conditions and after ca. 60 min saturation is reached. A final rinsing step removes loosely bound material and the resulting frequency shift can be used to estimate the adsorbed material according to the Sauerbrey equation that is applicable due to the rigidity of the surfaces.

As expected, there is some difference in the amount of deposited nanoparticles on the surfaces between the two methods (Fig. 3), whereby the covalent linking seems to be rather inefficient with a Δf_3 of ca. -5 ± 1 Hz (ca. 80 ng/cm^2 acc. to Sauerbrey). However, the electrostatic approach leads to an increased but still rather low adsorption of the nanoparticles onto the surface, with a Δf_3 of ca. -12 ± 2 Hz (ca. 210 ng/cm^2 acc. to Sauerbrey).

3.4. Antibacterial activity toward gram negative bacteria of immobilized S-Chi@Au nanoparticles

In order to estimate the antimicrobial activity of the surfaces, *E. coli* MG 1655 [R1-16] was chosen as model bacteria. The

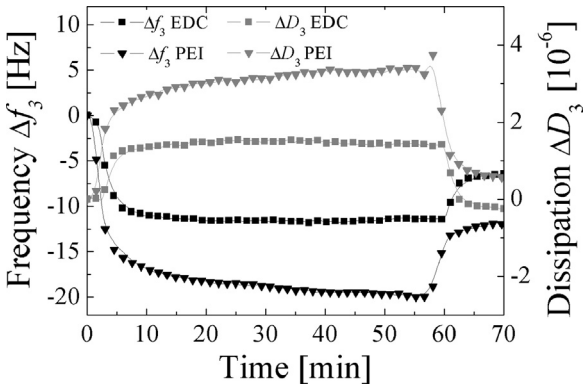

Fig. 3. Immobilization of S-Chi@Au using electrostatic deposition (PEI) and covalent attachment (EDC) monitored by QCM-D. Each adsorption experiment was performed in three parallels.

proliferation and shape of bacteria on the surfaces was visualized by scanning electron microscopy (Fig. 4). As shown in the SEM images in Fig. 4, the membranes of the bacteria exposed to S-Chi@Au modified surfaces are disintegrated and lyzed cells are observed. In contrast, unmodified surfaces (data not shown) show vital cells forming a biofilm in the early stage. An interesting feature on the SEM images is the observation of pili, which are characteristic for gram-negative bacteria (Mattick, 2002). pili are composed of proteins, which have several different functions for bacteria. They allow for horizontal gene transfer between individual bacteria cells (conjugative pili), which is probably one reason for the development of bacterial resistances toward antibiotics. On the other hand, they also provide motility of bacteria on surfaces using a hook-like mechanism (Type IV-pili). Pili that are visible on these SEM images are presumably conjugative pili. Plasmid R1-16 is derepressed meaning that DNA transfer genes are expressed in all cells. One of the transfer genes encodes pilin, pili are pilin polymerfibers. Conjugative pili (or F- or sex-pili) of this type are long (>2 μm and up to 20 μm in length), thin (10 nm in diameter) and feature flexible surface appendages. There are typically 1–5 pili per cell, they may appear thicker if wound around each other (Arutyunov & Frost, 2013). Three cells that form pili are enlarged (30,000×) in Fig. 4.

3.5. Anticoagulant activity of immobilized S-Chi@Au nanoparticles

Although the immobilized amount of nanoparticles is much smaller than expected, we investigated their anticoagulant effect toward citrated blood plasma. For this purpose, a QCM-D with specially designed open chambers for blood plasma addition has been employed. The QCM-D method has shown to provide a useful tool for a fast assessment of anticoagulant activity on surfaces due to the ability to follow fibrin formation on surfaces (frequency channel) and to monitor viscoelastic changes during the coagulation process (dissipation channel; conversion of fibrinogen to fibrin) (Andersson et al., 2005). In addition, the method is capable to determine the two phases of the last step in the coagulation of blood plasma, namely the prothrombin formation time and the fibrin clotting time. Since QCM-D is a method able to track changes in mass online, the fibrin deposition rate can be determined, which has been proven to be a good parameter for unspecific protein adsorption causing clots in real systems (Jung et al., 2009; Müller et al., 2010). Fig. 5 compares the total coagulation times (TCT) of the two surfaces that have been rendered with S-Chi@AuNPs. In fact, an increase of the coagulation times is observed compared to the uncoated surfaces (compare TCT of CMC: 4 min, PEI: <1 min). However, it can be clearly seen

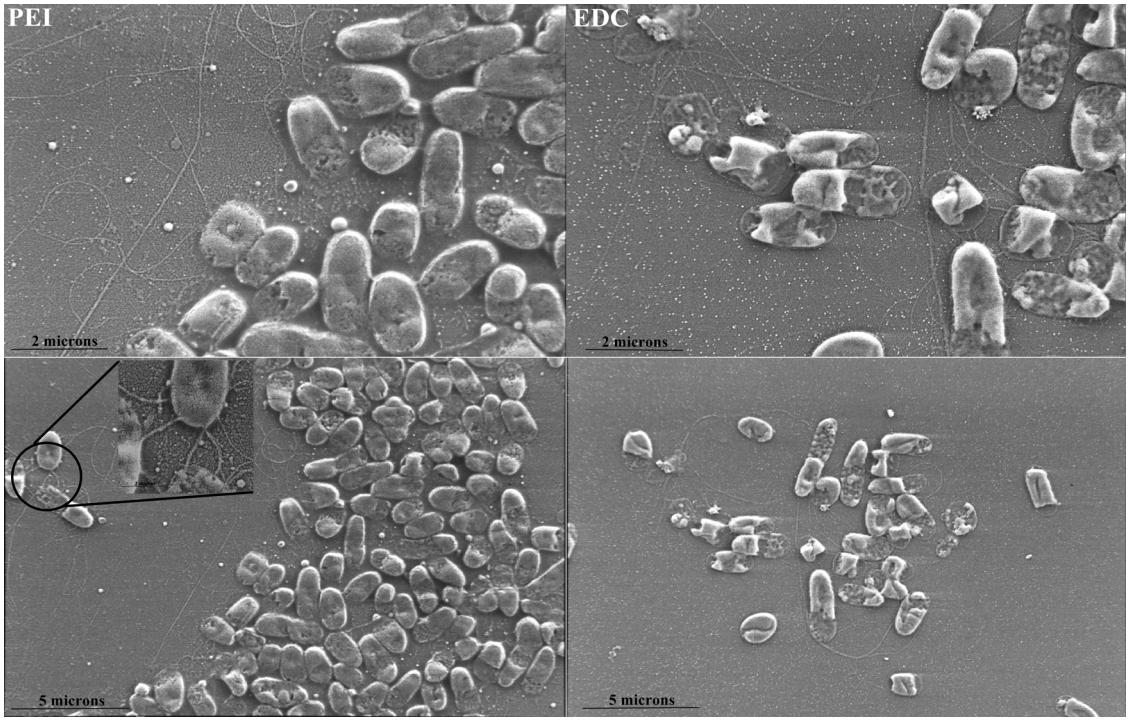

Fig. 4. Antibacterial activity of S-Chi@Au treated surfaces using SEM in different magnifications. The circle highlights the formation of pili between bacteria cells.

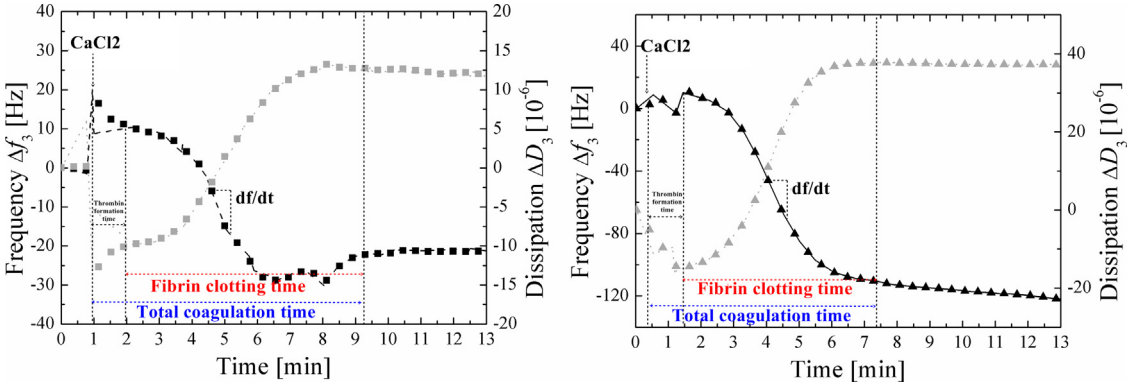

Fig. 5. Coagulation times of citrated blood plasma (triggered by $CaCl_2$) monitored online by the change in Δf_3 and ΔD_3 in a QCM-D experiment at 37 °C. Left: S-Chi@Au/PEI, Right: S-Chi@Au/EDC. Each coagulation experiment was performed in three parallels.

that the coagulation times are slightly different for both surfaces and correlate with the amount of particles on the surfaces (TCT: S-Chi@Au via covalent binding (EDC): 6.9 ± 0.2 min, via electrostatic binding (PEI): 8.2 ± 0.9 min). However, in terms of protein adsorption, there is a huge difference between the two surfaces. The EDC anchored particles lead to a higher frequency shift during coagulation than those immobilized by the PEI route (Δf_3: −110 ± 7 Hz, via EDC vs. −22 ± 10 Hz via PEI). In a similar manner, the fibrin deposition rates (d*f*/d*t*), which can be determined at the inflection point of the coagulation curves, are rather different with values of −34 ± 7 Hz/min (via EDC) and −18 ± 8 Hz/min (via PEI), which is much faster than those for heparinized PET surfaces (−2.3 Hz/min) (Doliska et al., 2012). Probably, the incompletely covered underlying substrate (EDC/CMC and PEI) is the origin for this behavior. The AuNPs deposited via the electrostatic approach on PEI leads to fibrin deposition similar to those reported for the S-Chi@AgNP related system (Breitwieser et al., 2013b). It should be mentioned that the contact of blood plasma with untreated PEI surfaces does not only induce immediate clotting (some seconds) but a detachment of the whole film from the QCM sensors as well, which is indicated by a huge positive frequency shift (ca. 1200 Hz, data not shown). Nevertheless, such a behavior has not been observed in any measurement for the surfaces, where S-Chi@AuNPs are immobilized onto the PEI surface. An overview is given in Table 2.

Table 2
Summary of data from coagulation times of citrated blood plasma (triggered by $CaCl_2$) of different surfaces.

	$\Delta f_3/3$ [Hz]	d*f*/d*t* [Hz/min]	TCT [min]
Au@S-Chi/CMC/EDC	−110 ± 7	−34 ± 7	6.9 ± 0.2
Au@S-Chi/CMC/PEI	−22 ± 10	−18 ± 8	8.2 ± 0.9
PEI	+1200 (detachment)	–	Immediate
CMC	−105 ± 9	−53 ± 11	3.8 ± 0.4

A comparison with other available materials (polymethylmethacrylate, polydimethylsiloxane, PET) that have been tested by QCM-D for such a purpose clearly shows that protein adsorption is much higher (Δf_3: −550 (PMMA), −750 (PDMS) and −1400 Hz (PET) (Andersson et al., 2005)) but also coagulation times are much

longer than those investigated in this study. However, a direct comparison is difficult due to some variations in the implementation of the test (e.g. measurement at 22 °C, way how coagulation was triggered). Recently, PET surfaces modified with heparins and sulfated dextrans using the same test setup as described in this study have been investigated (Doliska et al., 2012). A frequency shift (Δf_3) of ca −130 Hz was determined for neat PET surfaces (37° C) having a TCT of ca. 5 min, while rendering the PET surfaces via an electrostatic deposition of chitosan/heparin and chitosan/dextran sulfate prolongs TCT to 15 and 23 min, respectively. Nevertheless, Δf_3 is in the same range as for the surfaces described here.

4. Summary and conclusions

In this paper, we employed microwave assisted heating and an anticoagulant polysaccharide for the synthesis of gold nanoparticles. The crystalline AuNPs have a size of approximately 20 nm and feature a highly anticoagulant effect when contacted with whole blood due to the sulfated chitosan shell. Depending on the volume of added nanoparticle suspension, the aPTT of patients suffering from different diseases is doubled (from around 30 to ca. 70–80 s after addition of 0.25 μl nanoparticle suspension) and is nearly quadrupled (up to 117 s) if 0.50 μl nanoparticle suspension is added. The nanoparticles have been immobilized onto solid substrates, whereby highly antimicrobial action toward the employed test organism, *E. coli*, is realized as proven by SEM. The anticoagulant activity of the surfaces toward blood plasma has been investigated as well by a QCM-D method. Despite a rather low amount of adsorbed AuNPs, both surfaces exhibit prolonged coagulation times, which corroborates the findings from the determination of aPTT and PT that the core shell particles are highly efficient anticoagulants. However, in contrast to heparin, which features a rather specific role in the coagulation cascade, the underlying mechanism in the action of the nanoparticle system is rather unspecific. Probably, the combination between high surface charge and coordination of Ca^{2+} ions to the amine and sulfate groups of the polysaccharide shell of the nanoparticles mainly contribute to the anticoagulant activity. Nevertheless, the role of gold ions/atoms diffusing through the polysaccharide shell remains completely unclear. While in case of silver nanoparticles there is some discussion about their influence on coagulation, reports on the effect of gold are rare; currently there is not any evidence that pure gold nanoparticles influences the coagulation process.

Although the achieved anticoagulant activities are inferior to surfaces rendered with heparin for instance, the inclusion of antibacterial properties may allow the incorporation of such particle systems into anticoagulant coatings with possible use in preparation of catheters, dialysis tubings and blood sample tubes.

Acknowledgements

The Austrian Nano Initiative is gratefully acknowledged for its financial support (Nano Comp-Surf). The research leading to these results has received funding from the European Community's Seventh Framework Programme [FP7/2007–2013] under grant agreement no. 214015. Dr. Hubert Fasl is gratefully acknowledged for providing samples of chitosan sulfate.

References

Alexander, J. W. (2009). History of the medical use of silver. *Surgery Infections*, *10*, 290–292.

Andersson, M., Andersson, J., Sellborn, A., Berglin, M., Nilsson, B., & Elwinga, H. (2005). Quartz crystal microbalance-with dissipation monitoring (QCM-D) for real time measurements of blood coagulation density and immune complement activation on artificial surfaces. *Biosensors and Bioelectronics*, *21*, 79–86.

Arutyunov, D., & Frost, L. S. (2013). F conjugation: back to the beginning. *Plasmid*, *70*, 18–32.

Bergmann, A., Brunner-Popela, J., Fritz-Popovski, G., Früwirth, T., Glatter, O., Innerlohinger, J., et al. (1999). *PCG software package version 3.01.10*. (Copyright (c) 1999–2009).

Bergmann, A., Fritz, G., & Glatter, O. (2000). Solving the generalized indirect Fourier transformation (GIFT) by Boltzmann simplex simulated annealing (BSSA). *Journal of Applied Crystallography*, *33*, 1212–1216.

Bhattacharya, R., & Mukherjee, P. (2008). Biological properties of naked metal nanoparticles. *Advanced Drug Delivery Reviews*, *60*, 1289–1306.

Breitwieser, D., Moghaddam, M. M., Spirk, S., Baghbanzadeh, M., Pivec, T., Fasl, H., et al. (2013). In-situ preparation and characterization of silver nanocomposites on cellulosic fibers—microwave vs conventional heating. *Carbohydrate Polymers*, *94*, 677–686.

Breitwieser, D., Spirk, S., Fasl, H., Chemelli, A., Reichel, V. E., Kulterer, M. R., et al. (2013). Design of simultaneous antimicrobial and anticoagulant surfaces based on nanoparticles and polysaccharides. *Journal of Materials Chemistry B*, *1*, 2220–2230.

BrunnerPopela, J., & Glatter, O. (1997). Small-angle scattering of interacting particles.1. Basic principles of a global evaluation technique. *Journal of Applied Crystallography*, *30*, 431–442.

Cheng, F., Betts, J. W., Kelly, S. M., Schaller, J., & Heinze, T. (2013). Synthesis and antibacterial effects of aqueous colloidal solutions of silver nanoparticles using aminocellulose as combined reducing and capping reagent. *Green Chemistry*, *15*, 989–998.

Conlon, B. P., Nakayasu, E. S., Fleck, L. E., LaFleur, M. D., Isabella, M. D., Coleman, K., et al. (2013). Activated ClpP kills persisters and eradicates a chronic biofilm formation. *Nature*, *503*, 365–370.

Croes, S., Stobberingh, E. E., Stevens, K. N. J., Knetsch, M. L. W., & Koole, L. H. (2011). Antimicrobial and anti-thrombogenic features combined in hydrophilic surface coatings for skin-penetrating catheters. synergy of co-embedded silver particles and heparin. *ACS Applied Materials & Interfaces*, *3*, 2543–2550.

D'Costa, V. M., McGrann, K. M., Hughes, D. W., & Wright, G. D. (2006). Sampling the antibiotic resistome. *Science*, *311*, 374–377.

Davies, J., & Davies, D. (2010). Origins and evolution of antibiotic resistance. *Microbiology and Molecular Biology Reviews*, *74*, 417–433.

Doliska, A., Strnad, S., Stana, J., Martinelli, E., Ribitsch, V., & Stana-Kleinschek, K. (2012). In vitro haemocompatibility evaluation of PET surfaces using the quartz crystal microbalance technique. *Journal of Biomaterials Science Polymer Edition*, *23*, 697–715.

ECDC. (2012). *Surveillance of healthcare-associated infections in Europe*. Stockholm: European Centre for Disease Prevention and Control, 2007.

Ehmann, H., Spirk, S., Doliška, A., Mohan, T., Gössler, W., Ribitsch, V., et al. (2013). Generalized indirect Fourier transformation (GIFT) as a valuable tool for the structural characterization of nanocrystalline cellulose by small angle X-ray scattering. *Langmuir*, *29*, 3740–3748.

Fasl, H., Fras-Zemljic, L., Gössler, W., Stana-Kleinschek, K., & Ribitsch, V. (2012). Investigations into amphiphilic chitosan: Properties and availability of original and newly introduced functional groups. *Macromolecular Chemistry and Physics*, *213*, 1582–1589.

Fasl, H., Stana, J., Stropnik, D., Strnad, S., Stana-Kleinschek, K., & Ribitsch, V. (2010). Improvement of the hemocompatibility of PET surfaces using different sulphated polysaccharides as coating materials. *Biomacromolecules*, *11*, 377–381.

Fritz, G., Bergmann, A., & Glatter, O. (2000). Evaluation of small-angle scattering data of charged particles using the generalized indirect Fourier transformation technique. *Journal of Chemical Physics*, *113*, 9733–9740.

Gericke, M., Doliska, A., Stana, J., Liebert, T., Heinze, T., & Stana-Kleinschek, K. (2011). Semi-synthetic polysaccharide sulfates as anticoagulant coatings for PET, 1—Cellulose sulfate. *Macromolecular Bioscience*, *11*, 549–556.

Huang, H., & Yang, X. (2004). Synthesis of polysaccharide-stabilized gold and silver nanoparticles: A green method. *Carbohydrate Research*, *339*, 2627–2631.

Jung, H., Kim, J.-Y., Kim, Y., Tae, G., Kim, Y. H., & Johannsmann, D. (2009). QCM and AFM analysis of anticoagulant activities of sulfonated polymers against fibrin formation. *Langmuir*, *25*, 7032–7041.

Khan, M. S., Vishakante, G. D., & Siddaramaiah, H. (2013). Gold nanoparticles a paradigm shift in biomedical applications. *Advances in Colloid and Interface Science*, *199–200*, 44–58.

Koehler, S., Liebert, T., & Heinze, T. (2008). Interactions of ionic liquids with polysaccharides. VI. Pure cellulose nanoparticles from trimethylsilyl cellulose synthesized in ionic liquids. *Journal of Polymer Science Part A: Polymer Chemistry*, *46*, 4070–4080.

Lara, H. H., Garza-Treviño, E. N., Ixtepan-Turrent, L., & Singh, D. K. (2011). Silver nanoparticles are broad-spectrum bactericidal and virucidal compounds. *Journal of Nanbiotechnology*, *9*, 30.

Mattick, J. S. (2002). Type IV pili and twitching motility. *Annual Review of Microbiology*, *56*, 289–314.

Miller, J. H. (1977). *Experiments in molecular genetics*. Cold Spring Harbor, NY: Cold Spring Harbor Laboratory Press.

Mohan, T., Spirk, S., Kargl, R., Doliska, A., Vesel, A., Salzmann, I., et al. (2012). Exploring the rearrangement of amorphous cellulose model thin films upon heat treatment. *Soft Matter*, *8*, 9807–9815.

Mohan, T., Zarth, C., Doliska, A., Kargl, R., Grießer, T., Spirk, S., et al. (2013). Interactions of a cationic cellulose derivative with an ultrathin cellulose support. *Carbohydrate Polymers*, *92*, 1046–1053.

Müller, L., Sinn, S., Drechsel, H., Ziegler, C., Wendel, H.-P., Northoff, H., et al. (2010). Investigation of prothrombin time in human whole-blood samples with a quartz crystal biosensor. *Analytical Chemistry*, *82*, 658–663.

Sacarescu, L., Simionescu, Mihaela, & Sacarescu, G. (2011). Pseudo-template synthesis of gold nanoparticles based on polyhydrosilanes. *Applied Surface Science*, *257*, 3236–3242.

Sauerbrey, G. (1959). Verwendung von Schwingquarzen zur Wägung dünner Schichten und zur Mikrowägung. *Zeitschrift fur Physiotherapie*, *155*, 206–222.

Schlücker, S. (2009). SERS microscopy: Nanoparticle probes and biomedical applications. *ChemPhysChem*, *10*, 1344–1354.

Vikhoreva, G., Bannikova, G., Stolbushkina, P., Panov, A., Drozd, N., Makarov, V., et al. (2005). Preparation and anticoagulant activity of a low-molecular-weight sulfated chitosan. *Carbohydrate Polymers*, *62*, 327–332.

Wagner, M. A., Zahrl, D., Rieser, G., & Koraimann, G. (2009). Growth phase- and cell division-dependent activation and inactivation of the σ32 Regulon in *Escherichia coli*. *Journal of Bacteriology*, *191*, 1695–1702.

Weyerich, B., Brunner-Popela, J., & Glatter, O. (1999). Small-angle scattering of interacting particles. II. Generalized indirect Fourier transformation under consideration of the effective structure factor for polydisperse systems. *Journal of Applied Crystallography*, *32*, 197–209.

Williams, A., & Ibrahim, I. T. (1981). Carbodiimide chemistry: recent advances. *Chemical Reviews*, *81*, 589–636.

Zahrl, D., Wagner, M., Bischof, K., & Koraimann, G. (2006). Expression and assembly of a functional Type IV secretion system elicit extracytoplasmic and cytoplasmic stress responses in *Escherichia coli*. *Journal of Bacteriology*, *188*, 6611–6621.